Protein Science (2000), *9*:158–169. Cambridge University Press. Printed in the USA.

A step toward the prediction of the fluorescence lifetimes of tryptophan residues in proteins based on structural and spectral data

ALAIN SILLEN, JOSÉ FERNANDO DÍAZ, AND YVES ENGELBORGHS

Laboratory of Biomolecular Dynamics, University of Leuven, Celestijnenlaan 200D, B-3001 Leuven, Belgium

(RECEIVED August 10, 1999; FINAL REVISION October 29, 1999; ACCEPTED November 5, 1999)

Abstract

A method is presented that allows the calculation of the lifetimes of tryptophan residues on the basis of spectral and structural data. It is applied to two different proteins. The calcium binding protein from the sarcoplasm of the muscles of the sand worm *Nereis diversicolor* (NSCP) changes its conformation upon binding of Ca^{2+} or Mg^{2+}. NSCP contains three tryptophan residues at position 4, 57, and 170, respectively. The fluorescence lifetimes of W57 are investigated in a mutant in which W4 and W170 have been replaced. The time resolved fluorescence properties of W57 are linked to its different microconformations, which were determined by a molecular dynamics simulation map. Together with the determination of the radiative rate constant from the wavelength of maximum intensity of the decay associated spectra, it was possible to determine an exponential relation between the nonradiative rate constant and the distance between the indole CE3 atom and the carbonyl carbon of the peptide bond reflecting a mechanism of electron transfer as the main determinant of the value for the nonradiative rate constant. This result allows the calculation of the fluorescence lifetimes from the protein structure and the spectra. This method was further tested for the tryptophan of Ha-ras p21 (W32) and for W43 of the Tet repressor, which resulted in acceptable values for the predicted lifetimes.

Keywords: molecular dynamics simulations; nonradiative rate constant; protein dynamics; radiative rate constant

Tryptophan is a naturally occurring fluorescent probe present in most proteins that is sensitive to its immediate environment. Therefore, it can be used to study structural and dynamic properties of proteins. However, this necessitates an exact knowledge of the relation between the fluorescence properties and the protein environment. In proteins, tryptophan fluorescence usually displays a multi-exponential decay. This is either the consequence of excited state reactions or of the existence of different microconformations of tryptophan (Dahms et al., 1995). This makes it difficult to relate fluorescence properties with structure, because usually only one local conformation of tryptophan is known from the structure determination by X-ray analysis and only a few by NMR analysis. In this work, we present a method to identify the different microconformations and calculate the associated decay constants. The main fluorescence properties of tryptophan are the fluorescence lifetime, which is determined by the radiative and nonradiative rate constant, the emission spectrum, which is characterized by the wavelength of maximum emission intensity, and its fluorescence intensity, and the quantum yield. The wavelength of maximum emission and the radiative rate constant is strongly related to the electric field in the vicinity of the tryptophan (Szabo & Faerman, 1992; Callis & Burgess, 1997). In this paper, we present an easy way to calculate the radiative rate constant from the wavelength of maximum emission. This creates the possibility to calculate the radiative rate constant for individual lifetimes. With the information of the radiative rate constant and the fluorescence lifetime, the nonradiative rate constant of the individual lifetimes can be calculated. To determine the different microconformations of tryptophan, the χ_1 and χ_2 angles of tryptophan are set at 9×6 different values in the computer model. From these initial positions, a free molecular dynamics simulation is started to explore the conformational space. For the resulting microconformations the nonradiative rate constant can be explained by means of an exponential relation between the nonradiative rate constant and the distance between the CE3 atom of tryptophan and the carbonyl carbon of the peptide bond, based on the theory of electron transfer. Also the relative populations of the different microconformations can be related to the amplitude fraction of the different lifetimes. We have applied this method to three different proteins.

NSCP is the calcium binding protein isolated from the sarcoplasm of the muscles of the sand worm *Nereis diversicolor* and has

Reprint requests to: Yves Engelborghs, Celestijnenlaan 200D, B-3001 Leuven, Belgium; e-mail: yves.engelborghs@fys.kuleuven.ac.be.

Abbreviations: NSCP, Nereis sarcoplasmic calcium binding protein; SCP, sarcoplasmic calcium binding protein; IPTG, isopropyl β-D-thiogalactoside; MD, molecular dynamics; k_{nr}, nonradiative rate constant; k_r, radiative rate constant; DAS, decay associated spectra; PDB, Protein Data Bank.

174 amino acids (Collins et al., 1988) with a relative molecular mass of 19,485. The three-dimensional X-ray structure (at 2 Å resolution) of Ca^{2+} bound NSCP (Fig. 1) is described by Vijay-Kumar and Cook (1992). NSCP has four domains with the typical EF-hand (Kretsinger & Nockolds, 1973) Ca^{2+} binding sequence, but only sites I, III, and IV can bind Ca^{2+} or Mg^{2+}. The protein has a compact structure with a central hydrophobic core of 20 amino acids, most of which are aromatic. The domains I and II form a pair by a back-to-back β-sheet just like the pair III and IV. NSCP is mainly α-helical (58%) with eight helices (A through H). It contains three tryptophan residues at position 4, 57, and 170, respectively. Our method was applied to a mutant containing only W57.

The result obtained for NSCP was further tested on an other protein, i.e., Ha-ras-p21, where a tryptophan was engineered by site directed mutagenesis at position 32. Ha-ras-p21 belongs to the *ras*-related superfamily of GTP-binding proteins, which is a family of small 20–25 kDa proteins that bind guanine nucleotides very tightly and cycle between an inactive guanosine diphosphate (GDP)-bound state and an active guanosine triphosphate (GTP)-bound state. These proteins are involved in the signal transmission pathway (Wittinghofer & Pai, 1991). As with the other G-proteins, GTP is bound in the active state of Ha-ras-p21, and to switch to the inactive state, the γ-phosphate of the nucleotide has to be hydrolyzed and released, while the GDP remains bound to the protein. Both states show differences in certain areas of the molecule (Pai et al., 1990; Tong et al., 1991) that lead to two different conformational states: the GTP-bound form and the GDP-bound form. In the active conformation, these proteins interact with an effector molecule. The GTPase activity on its own can be influenced by several effectors as guanosine triphosphatase activating proteins (GAPs) (Adari et al., 1988).

We have used a fluorescent mutant of p21 (Y32W). The tryptophan fluorescence yield of this mutant is significantly smaller (by ~45%) when GTP is bound as compared to the GDP-bound state (Rensland et al., 1995). The conformation (and fluorescence) of the GTP-state can also be obtained by the binding of BeF_3^- with the advantage that the GTP state is now a stable state (Díaz et al., 1997a). The structure of the mutant does not show any disturbance in comparison with the wild-type (Rensland et al., 1995). Finally, the method was also applied to literature data about W43 of the tet repressor protein with good results (Antonini et al., 1997).

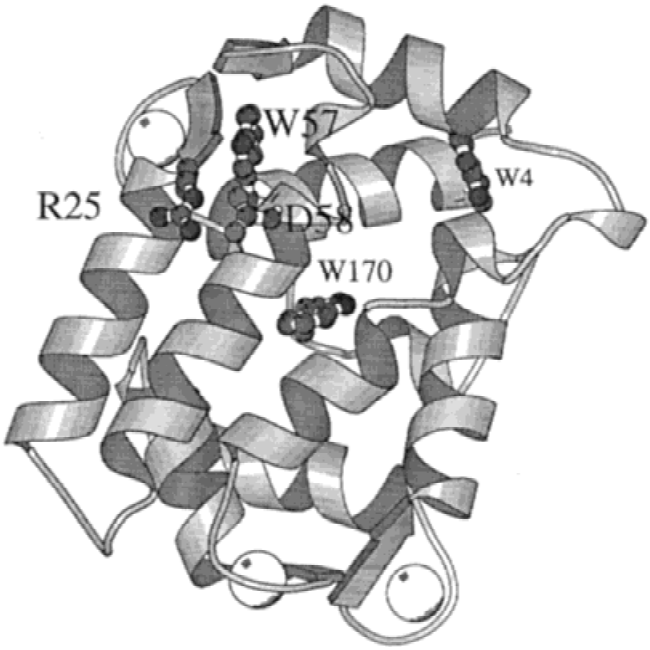

Fig. 1. MOLSCRIPT representation (Kraulis, 1991) of the X-ray structure of NSCP Ca^{2+}. The white spheres represent the calcium ions.

Results

Fluorescence spectra and quantum yields of the NSCP variants

Analysis of the fluorescence spectra (Fig. 2) and the quantum yields (Table 1) of NSCP variants that where measured in Ca^{2+} bound and apo state reveals that the quantum yield of W57 decreases strongly if Ca^{2+} is bound, also a change in the molar absorption coefficients is observed. The quantum yield of W57 decreases from 0.14 to 0.03 upon the binding of Ca^{2+}. The fluorescence of W57 is also strongly influenced by the salt bridge R25-D58 in the environment of W57 (Fig. 1). It is interesting to note that the molar absorption coefficients of individual tryptophans at 295 nm can vary between 2,338 and 3,194, while the molar absorption coefficient at 280 nm is much more constrained (Mach et al., 1992).

Time-resolved fluorescence parameters

The measurements were performed at emission wavelengths ranging from 320 to 380 nm in 10 nm intervals. A single or double exponential fit to the phase data yielded unacceptable high values of χ_R^2 and a significant nonrandomness in the autocorrelation function of the weighted residuals as a function of the frequency. Best fit with lowest χ_R^2 and no systematic deviations in the autocorrelation function of the weighted residuals is obtained with a triple or

Table 1. *Molar absorption coefficients, quantum yield, average lifetime, and radiative rate constant of NSCP and variants*

	ϵ_{295} (M^{-1} cm^{-1})	Q	$\langle\tau\rangle$ (ns)	$\langle k_r\rangle$ (ns^{-1})	λ_{max} (nm)
		W4-170F			
Ca	2,338 ± 198	0.033 ± 0.001	0.61	0.054	317
Mg	2,501 ± 321	0.032 ± 0.001	0.59	0.054	324
apo	2,957 ± 152	0.14 ± 0.01	3	0.048	330
		W4-170F/R25D			
Ca	2,878 ± 398	0.10 ± 0.02	2.2	0.046	336
Mg	2,984 ± 473	0.09 ± 0.01	2	0.046	336
apo	3,142 ± 357	0.13 ± 0.06	2.8	0.046	345
		W4-170F/R25D/D58R			
Ca	2,873 ± 45	0.12 ± 0.01	2.5	0.048	325
Mg	2,673 ± 47	0.08 ± 0.01	1.5	0.052	323
apo	3,194 ± 38	0.18 ± 0.01	3.4	0.052	328

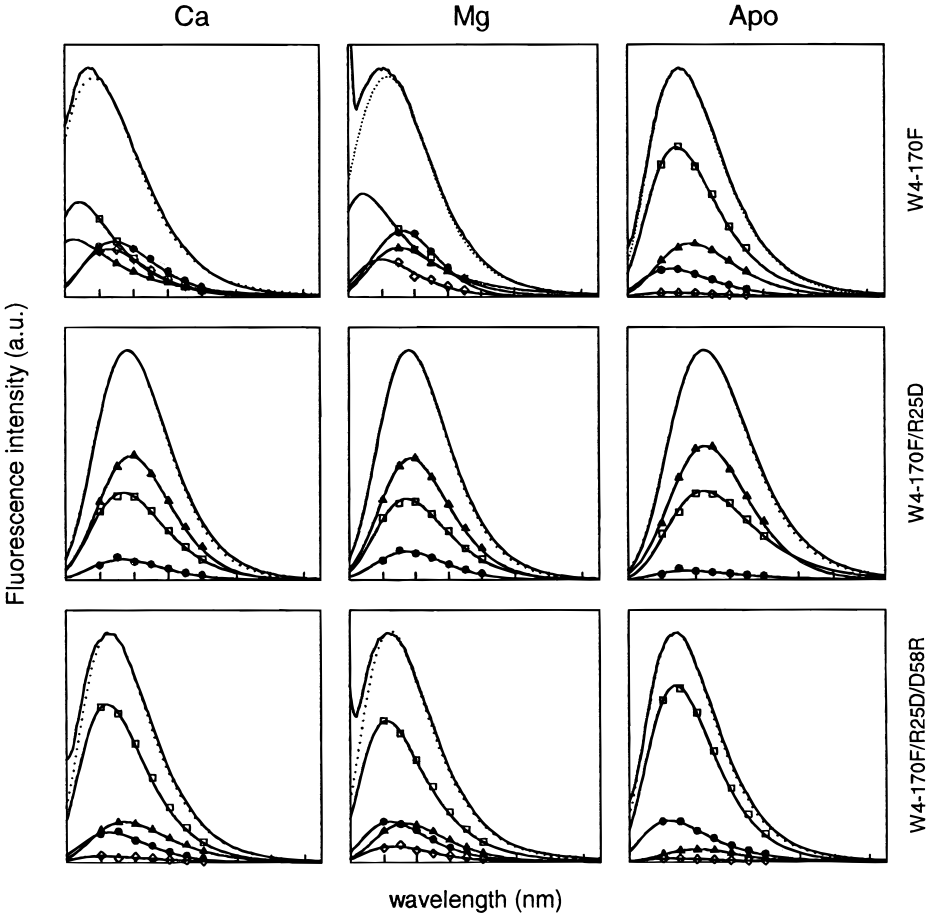

Fig. 2. Normalized decay associated spectra (DAS) of W4-170F, W4-170F/R25D, and W4-170F/R25D/D58R in the Ca^{2+}, Mg^{2+}, and apo form. Key to plot: ▲, longest lifetime; □, second longest lifetime; ●, middle lifetime; ◇, smallest lifetime; ...., sum of the decay associated spectra.

quadruple exponential function. We did not observe any dependency of the lifetimes on the emission wavelength. Therefore, to improve the quality of the decay parameters, a global analysis of all the phase measurements at the different wavelengths was performed. The results of this global fit are summarized in Table 2.

Relation between the radiative rate constant and the electric field in the vicinity of the indole ring

Szabo and Faerman (1992) suggested that the radiative rate constant is influenced by the electric field in the vicinity of the indole ring. The electric field over the indole ring is directly related with the wavelength of maximum emission intensity (Callis & Burgess, 1997). The relation between the emission spectrum and the radiative rate constant is given by the following equation (Strickler & Berg, 1962):

$$k_r = \left[2.88 \times 10^{-9} n^2 \frac{g_a}{g_b} \int \frac{\epsilon(\bar{\nu})}{\bar{\nu}} d\bar{\nu} \right] \frac{\int I(\bar{\nu})\, d\bar{\nu}}{\int \bar{\nu}^{-3} I(\bar{\nu})\, d\bar{\nu}}$$

$$= 2.88 \times 10^{-9} n^2 \frac{g_a}{g_b} g(absL_a) \cdot f'(\lambda_{\max}) \quad (1)$$

Table 2. *Lifetimes (τ), wavelength independent amplitude fraction (α), and χ_R^2 as obtained by global analysis of the fluorescence decay of NSCP mutant W4-170F in the Ca^{2+} bound state*

α_1	τ_1 (ns)	α_2	τ_2 (ns)	α_3	τ_3 (ns)	α_4	τ_4 (ns)	χ_R^2
0.66 ± 0.06	0.19 ± 0.08	0.23 ± 0.03	0.66 ± 0.20	0.09 ± 0.01	2.4 ± 0.3	0.02 ± 0.07	5.8 ± 0.3	3

where n is the refractive index of the medium; g_a and g_b are the degeneracies of the lower and upper state, respectively; ϵ is the molar absorption coefficient; $\bar{\nu}$ is the wave number; I is the fluorescence intensity. The factor behind the square brackets $f'(\lambda_{max})$ is responsible for the influence of the emission spectrum on the radiative rate constant. Using the lognormal function (Equation 10) for the shape of the spectra, this factor is fully determined by its dependence on the wavelength of maximum emission intensity. We constructed a pragmatic equation that allows an easy calculation of this factor from the wavelength of maximum emission intensity. We obtained 21 values of this factor by numerical integration of 21 different spectra of tryptophan, constructed with the lognormal function (Equation 10) with wavelengths of maximum intensity ranging from 310 to 355 nm. The results were then fitted to a sixth power polynomial (power six turned out to give the best fits):

$$f(\lambda_{max}) = a\lambda_{max}^6 + b\lambda_{max}^5 + c\lambda_{max}^4 + d\lambda_{max}^3 + e\lambda_{max}^2 + f\lambda_{max} + g \quad (2)$$

yielding the following values for the parameters: $a = -3.6985\text{E}{-12}$, $b = 7.6207\text{E}{-09}$, $c = -6.5369\text{E}{-06}$, $d = 2.9880\text{E}{-03}$, $e = -0.7675$, $f = 104.9553$, $g = -5{,}960.8610$.

Taking 1.5 for the refractive index of the protein (Desie et al., 1986) and adjusting the dimensions to ns^{-1} for k_r, Equation 1 becomes for tryptophan:

$$k_r = 6.48 \cdot 10^{-9} g(absL_a) f(\lambda_{max}) \quad (3)$$

where $g(absL_a)$ is the factor related to the absorption band L_a of tryptophan as defined in Equation 1. The L_a absorption band is very difficult to measure because it overlaps with the L_b absorption band (Valeur & Weber, 1977). Therefore an average factor is determined by fitting Equation 3 to the $\langle k_r \rangle$ obtained from the mutants W57-170F, W4-170F, W4-170F/R25D, and W4-170F/R25D/D58R, and a value of $(292 \pm 7) \cdot 10^4$ is obtained (Fig. 3). The last two mutants were made to remove and/or to invert the salt bridge (and therefore also the electric field) in the environment of W57. The data of Table 1 and Figure 2 clearly demonstrate these effects.

Energy mapping

Minimum perturbation map calculations of W57 were performed on the X-ray structure (PDB ID:2SCP). The energy map of W57 (Fig. 4) shows only one stable conformation for the tryptophan side chain, i.e., $\chi_1 = 180°$ and $\chi_2 = -100°$. This minimum energy conformation corresponds to the conformation found in the crystal as determined by X-ray analysis ($\chi_1 = 180°$ and $\chi_2 = -90°$).

Molecular dynamics of NSCP

In the energy minimized overall protein structure, the χ_1 and χ_2 angle of Trp57 are set at 54 different starting values. These were again energy minimized, heated, and equilibrated. Consequently, a normal molecular dynamics (MD) simulation of 50 ps was done to monitor the evolution of χ_1 and χ_2 angles of Trp57 at every starting position. Sixty-five percent of the starting positions resulted in a distortion of the secondary structure due to an energetically and/or geometrical very bad starting structure. The start and end values are summarized in Table 3. The final values of χ_1 and χ_2 for the conformation of the remaining 35% are shown in Figure 5. Although 19 start structures remain, there are only seven possible conformations of W57. Different starting structures converge to the same energetically favored conformations. Thus, the 120 ps MD in total explores enough conformational space to find the stable energy minima. The minimal potential energy U_0 (Schlitter et al., 1994) of the whole protein for the different conformations

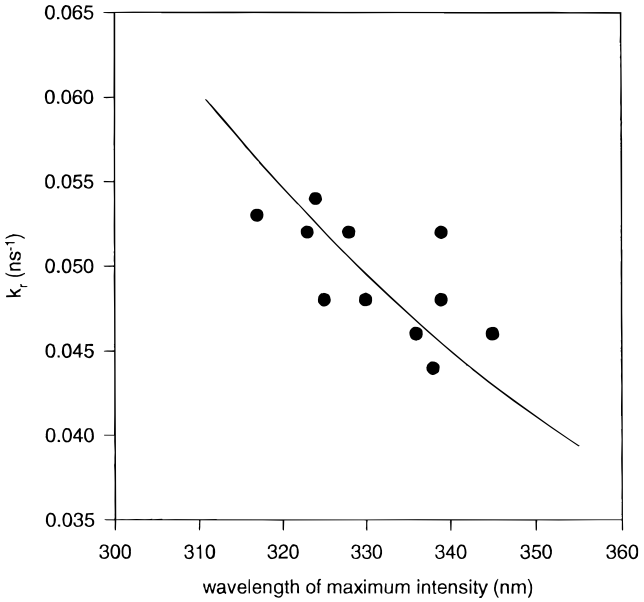

Fig. 3. The radiative rate constant as function of the wavelength of maximum intensity as fitted to Equation 13.

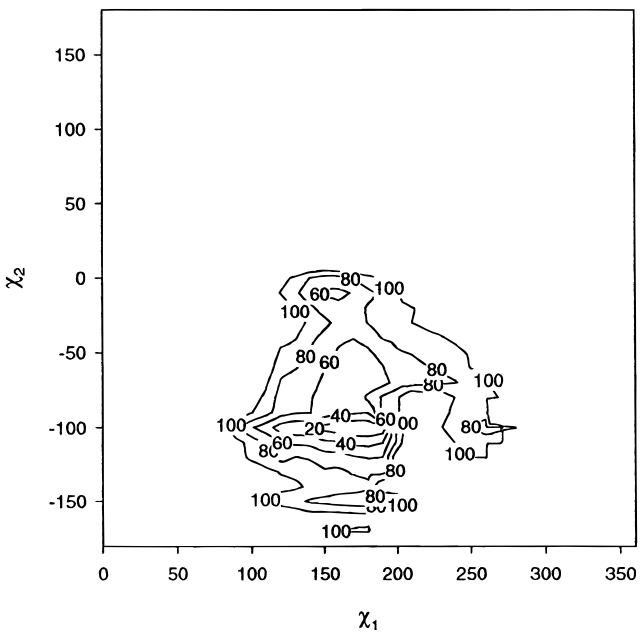

Fig. 4. Energy map of W57 in the NSCP Ca^{2+} conformation. The values have kcal/mol as unit and are relative to the lowest value.

Table 3. *Start and final values of χ_1 and χ_2 dihedral angles of Trp57 after a 50 ps molecular dynamics simulation*[a]

	Start χ_1								
	−180	−140	−100	−60	−20	20	60	100	140
Start	**Final χ_1/χ_2**								
χ_2: 120	−160/ −90 A	−70/ −70 X	−170/ −110 A	140/ 0 D	170/ 160 X	170/ 90 X	−180/ −70 X	−170/ −70 X	180/ −120 X
χ_2: 60	−160/ −120 X	−160/ −110 A	−80/ −90 C	−160/ −90 X	−70/ −40 X	20/ −70 X	160/ 120 B	160/ 120 B	120/ 80 X
χ_2: 0	−170/ 90 X	−160/ −120 A	−160/ −120 X	40/ 40 X	40/ −80 X	70/ −130 X	170/ 160 B	150/ 120 B	170/ 160 B
χ_2: −60	170/ 180 B	−170/ 70 X	−50/ 90 X	30/ 80 X	60/ 20 X	80/ −20 C′	70/ −70 X	−70/ 100 X	170/ 170 B
χ_2: −120	170/ 150 B	180/ 170 B	70/ −100 X	−60/ 120 X	60/ 20 X	−50/ 130 X	−50/ 120 B′	160/ −10 X	170/ 160 B
χ_2: −180	170/ −20 X	100/ −100 B″	−80/ 60 X	70/ −170 X	70/ 90 X	50/ 30 X	−40/ 110 X	−180/ −120 X	160/ −30 X

[a]A through D different families of microconformations:

A: $-170 < \chi_1 < -160$; $-120 < \chi_2 < -90$
B: $150 < \chi_1 < 180$; $120 < \chi_2 < 180$, B′: $\chi_1 \approx -50$; $\chi_2 \approx 120$, B″: $\chi_1 \approx 100$; $\chi_2 \approx -100$
C: $\chi_1 \approx -80$; $\chi_2 \approx -90$, C′: $\chi_1 \approx 80$; $\chi_2 \approx -20$
D: $\chi_1 \approx 140$; $\chi_2 \approx 0$
X: Start conformation distorts secondary structure.

is the same within 5%. To estimate the relative population of a certain local conformation, the number of initial positions from which this final conformation can be reached is calculated. Conformation B, for example, is 10 times reached out of 19 starting positions (Table 3); hence, conformation B is assumed to have a 53% chance of occurring and its relative population is therefore also 53% (Table 4). In the immediate neighborhood of W57, none of the known quenchers (Chen & Barkley, 1998) are found. Therefore, the only possible quenching mechanism seems to be electron transfer to the peptide bond (Chen et al., 1996; Antonini et al., 1997). Therefore, the distance to the carbonyl carbons of the peptide backbone in the vicinity of W57 are calculated and are shown in Table 4. Conformations with the same distance to the carbonyl carbon are collected in the same family because they should have the same lifetime (Table 4). The population of these families can then be compared with the amplitude fraction of the different lifetimes of the W4-170F variant (Table 4).

Correlation between the different conformations and the fluorescence lifetimes of p21

In the protein p21-GDP, Trp 32 is set to the six conformational energy minima of free Trp (Gordon et al., 1992) for χ_1: +60°, −180°, and −60° combined with χ_2: +90° and −90°, from where

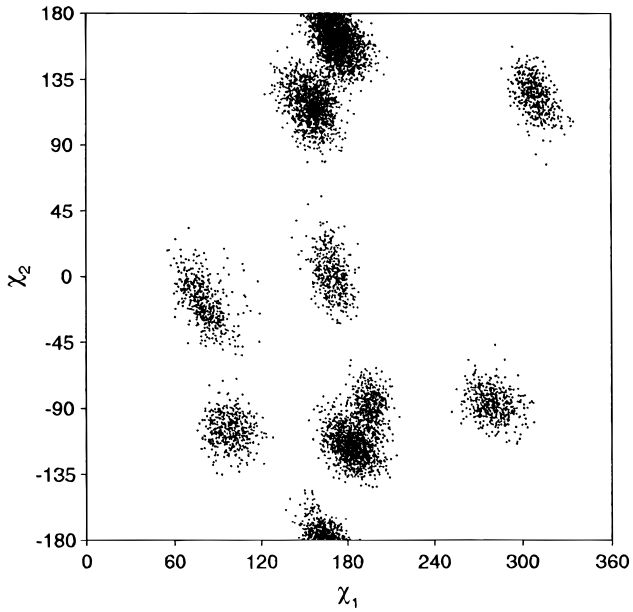

Fig. 5. Possible conformations of W57 in NSCP Ca^{2+} conformation, determined by a free MD scan (see text). The dots represent the χ_1 and χ_2 angles of W57.

Table 4. *Fraction of population and distance between W57(CE3) and the carbonyl carbon of the peptide bond of the different conformations of W57 in NSCP*

Native conformation	Global family	Fraction (%) conformation	Fraction (%) global family	Distance to 57(C) (Å)	Distance to 56(C) (Å)	Associated lifetime (amplit fraction)
A	A	21	21	**4.5**	5.8	τ_2 (0.23)
B	B	53	63	**3.8**	5.8	τ_1 (0.66)
B′	B	5		4.8	**3.7**	
B″	B	5		**3.7**	6.3	
C	C	5	10	5.6	**5**	τ_3 (0.09)
C′	C	5		**5.1**	6.4	
D	D	5	5	**5.5**	5.7	τ_4 (0.02)

an energy minimization and a 200 ps molecular dynamics simulation was started. The averaged values over the 200 ps of the distances between Trp32 and the carbonyl of the backbone are shown in Table 5. The conformation with starting value χ_1:−180° and χ_2:+90° changes its conformation to the χ_1:−60° and χ_2:+90° conformation, indicating that the χ_1:−180° and χ_2:+90° conformation is an unstable one. The lifetimes of p21 at 22 °C where τ_1 = 0.3, τ_2 = 1.8, and τ_3 = 4.9 the measured average radiative rote constant was 0.041 ns^{-1}.

Quenching of the fluorescence of p21 Y32W in the GDP and GDP + BeF_3^- state with Cu^{2+} and I^-

To determine the solvent accessibility and the charge of the environment of the species with different lifetimes of Trp32, a quenching study is performed with Cu^{2+} and I^- and the results are shown in Table 6. The quenching constants of the different lifetimes indicate that the microstate associated with the middle lifetime is more solvent accessible than the microstate of the long lifetime. When the quenching constants in the presence and absence of BeF_3^- are compared, it becomes clear that the microstate of the middle lifetime is more solvent accessible in the absence of BeF_3^- while the microstate of the longer lifetime is more solvent accessible in the presence of BeF_3^-.

Table 5. *Distance (Å) between atom CE3 of Trp32 and the C atom of the carbonyl groups of the amino acids 30 to 33 in the different microconformations of W32 in the GDP state structure of the Y32W variant*

	For χ_2 = +90		
χ_1	+60	−60	
D30	4.9372 ± 0.5769	8.0895 ± 0.5496	
E31	4.1738 ± 0.4377	5.6872 ± 0.3167	
W32	5.0423 ± 0.2192	4.3806 ± 0.3496	
D33	7.0633 ± 0.2680	5.0548 ± 0.7320	
	For χ_2 = −90		
χ_1	+60	−180	−60
D30	7.9112 ± 0.3297	6.2418 ± 0.7713	4.2802 ± 0.4607
E31	6.4160 ± 0.1869	4.5683 ± 0.4951	4.7448 ± 0.4161
W32	4.1341 ± 0.2905	5.1135 ± 0.3339	5.5644 ± 0.1790
D33	3.8668 ± 0.2320	7.1474 ± 0.5124	7.4092 ± 0.3209

Discussion

The fluorescence decay of a single tryptophan residue in a protein is usually multi-exponential. The origin of this complex behavior is a matter of discussion. Basically two classes of explanations are offered. They either belong to a dynamic picture, i.e., a collection of excited state reactions, or to a static picture, i.e., a multiplicity of conformational states of the residue (conformers or rotamers). Examples of support exist for each mechanism, and it is quite clear that both explanations are necessary to describe the complex behavior of tryptophan residues in proteins. Moreover, the static model has to be expanded with the kinetics of interchange between the different conformers of tryptophan to complete the picture. The different excited state reactions that are possible for a tryptophan in a protein have been reviewed by Chen and Barkley (1998). They include intersystem crossing, solvent quenching, excited state proton, and electron transfer. The balance of the different possibilities and the rate constants differ for the aminoacid side chains to be considered. All these processes are parallel pathways of deactivation, and therefore they do not explain in se the existence of different lifetimes for a single tryptophan, unless they are coupled to the existence of different conformers of the residue. Other excited state processes, such as energy transfer and solvent or protein

Table 6. *Bimolecular quenching constants k_q determined for the middle and long lifetime of Trp32 in the GDP and GDP + BeF_3^- state of Y32W*

	k_q (ns^{-1} M^{-1})			
Nucleotide	GDP		GDP + BeF_3^-	
lifetime quencher	τ_2	τ_3	τ_2	τ_3
Cu^{2+}	1,246 ± 135	39 ± 1	270 ± 15	72 ± 5
I^-	0.53 ± 0.06	0.082 ± 0.004	0.43 ± 0.02	0.088 ± 0.006

relaxation, can be the origin of a multi-exponential fluorescence decay. Indications for these processes are negative amplitudes and emission wavelength dependent lifetimes.

Recently, a new model has been proposed by Hudson (1999). In this model, it is assumed that electron transfer can result in the formation of an ion-pair complex with a lifetime determined by its emission rate constant and a rate constant for return to the original excited state of tryptophan. This mechanism gives rise to the appearance of two exponentials, the amplitudes of which are determined in a complex way by the different rate constants involved. This fact allows for a diagnostic of this mechanism: changing the lifetimes of the excited states by adding an external quencher, e.g., acrylamide changes the ratio of the amplitudes, which would not be the case if the amplitudes reflected populations of different conformers (unless specific static quenching would be possible). This analysis has been successfully applied to T4-lysozyme (Harris & Hudson, 1990). In this single Trp protein, two lifetimes are observed, respectively, of 1 and 3 ns. The replacement of an amide by Ala in the immediate neighborhood of the tryptophan leads to a single lifetime of 5 ns. The formation of an electron transfer ion pair with the amide can explain the quenching and the production of the two lifetimes, and the amplitude ratio changes indeed with the concentration of added acrylamide.

We have studied W126 of the DsbA-mutant W76F (Sillen et al., 1999). We also replaced two amides in the immediate neighborhood of W126 one by one but we observed, however, an increased quenching in the absence of the amides and a reshuffling of the amplitudes (Sillen et al., 1999). Moreover, the kinetics of the reshuffling could be estimated to be very slow.

The question remains therefore of how to explain different lifetimes when no obvious quenching groups are available in the environment as is the case for W57 of NSCP.

As shown previously (Chen et al., 1996; Chen & Barkley, 1998), electron transfer to the peptide bond is also a candidate for quenching. The peptide bond is always present, also in the denatured state. Since electron transfer is strongly distance dependent, its efficiency will depend on the conformation of the Trp residue. Both through bond as well as through space electron transfer might have to be considered. We therefore decided to explore this possibility.

Molecular mechanics and dynamics simulations

To characterize these microconformations of tryptophan, minimum perturbation maps are calculated (Silva & Prendergast, 1996). These maps display areas where Trp is in an energetically favored position. But these maps do not take into account that changes of conformations of Trp in proteins are dynamic processes that occur at room temperature rather than at 0 K. Therefore, instead of calculating a minimum perturbation map, a different approach is taken here to calculate the different conformations of tryptophan. For W57 of NSCP there is an important difference between the energy map (Fig. 4) and the MD-conformation map (Fig. 5); the energy map predicts only one possible conformation for W57, whereas the MD-conformation map shows that different microconformations are possible. Fluorescence measurements of W57 also reveal four lifetimes. In the past the existence of only one energy minimum in the energy map was used as an argument against the idea that the different lifetimes of tryptophan originated from different conformations. Our MD results show that small changes in the backbone conformation can allow other conformations to exist that are not revealed in energy maps. To associate the different conformations to lifetimes, the distance between the indole and the carbonyl carbon of the peptide backbone is calculated. The smallest distance between the CE3 atom of tryptophan and the C atom of the carbonyl carbon of the peptide backbone is found to belong to four different classes $<$4, 4.5, $\sim$5.0, and 5.5 Å (Table 4), which are associated to the respective lifetimes τ_1, τ_2, τ_3, and τ_4. This assignment is based on two arguments: (1) the similarity between the chance of populating a certain microconformation and the amplitude fractions of the associated lifetime is very good (Table 4); (2) for this particular combination of lifetimes and microconformations, an exponential relation is obtained between k_{nr} (which can be calculated from the inverse of the measured lifetime and the k_r obtained by Equation 3) and the distance between CE3 of Trp and the carbonyl carbon of the peptide bond (Fig. 6). This exponential relation reflects the main dynamic quenching mechanism, which is electron transfer from atom CE3 of Trp to the carbonyl carbon of the peptide backbone (Chen et al., 1996; Antonini et al., 1997). Thus, this plot can be fitted by the following equation derived for electron transfer by Marcus and Sutin (1985):

$$k_{ET}(R) = k_0 \exp(-\beta(R - R_0)) \tag{4}$$

where $k_{ET}(R)$ is the rate for electron transfer, k_0 is the rate of electron transfer at the van der Waals contact distance ($R_0 = 3$ Å), β is the range parameter that is depended on the medium. The fit yields $k_0 = 25 \pm 3$ ns^{-1} and $\beta = 1.9 \pm 0.1$ Å^{-1}.

The error on $k_{ET}(R)$ can be calculated from the derivative

$$dk_{ET}(R) = [k_0(-\beta)\exp(-\beta(R - R_0))\, dR]. \tag{5}$$

With $\beta = 1.9$ and dR around 0.3 Å as obtained from MD simulations, the relative error of $k_{ET}(R) = 60\%$. This error is probably largely overestimated because it assumes that emission from all R-values is equally likely, which is obviously not the case. It also

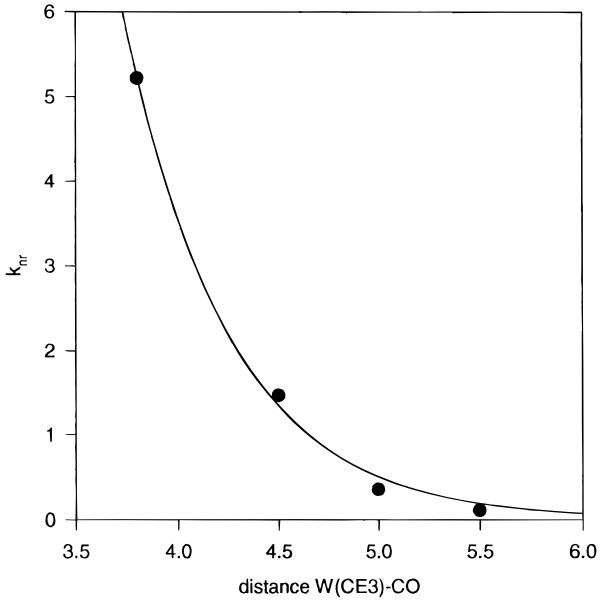

Fig. 6. The nonradiative rate constant as function of the distance between the CE3 atom of W57 and the C atom of the carbonyl of the peptide bond of W57.

suggests the possibility that these distance fluctuations are at the origin of lifetime distributions observed in the literature.

The same approach can be employed to determine the different conformations of W32 of p21. Also, here no pronounced quenchers are found around W32. Because W32 is largely solvent accessible, the solvent must be taken into account in this MD map. To speed up the procedure, because solvent simulations consume a much longer calculation time than vacuum ones, we limited the starting conformations to the six possible conformations observed in free tryptophan. These MD simulations reveal five possible conformations of W32 in p21. Applying Equation 4 to the distance between the closest peptide carbonyl carbon and CE3 of W32 yielded calculated lifetimes that were, however, very different to the measured ones. However, limiting the use of Equation 4 to only the carbonyl carbon of W32 itself yielded calculated lifetimes that where almost identical to the measured ones (Table 7) suggesting that maybe not every carbonyl carbon of the peptide bond is involved in the quenching. This restriction can also be applied to NSCP; if only the carbonyl carbon of W57 itself is used to determine the parameters of Equation 4, the same parameters are still obtained. To test the validity of Equation 4, we looked in the literature for data about a tryptophan where the lifetimes where measured and where the different conformations where determined. Testing Equation 4 to the data for W43 of the tet-repressor as determined by Antonini et al. (1997) yielded an acceptable correlation between the calculated and measured lifetimes (Table 7), taking into account that the conformations of this tryptophan was obtained by an energy map.

The question remains why only the carbonyl of tryptophan itself is a quencher and not other carbonyls. The rate of electron transfer is much larger through covalent bonds than through vacuum (Gray & Winkler, 1996; Wierzchowski, 1997). However, if the electron transfer propagates through the covalent bonds that connect the indole with its carbonyl then there would only be one lifetime. A possible explanation is that for efficient electron transfer the orbitals involved have to be correctly orientated toward each other (Wierzchowski, 1997). Thus, the distance dependency of the efficiency of electron transfer reflects in fact the effect of the orientation of the bonds involved, while for through space electron transfer the orientation is not determined by the distance.

The distribution of microconformations of a tryptophan is suggested to be largely determined by the secondary structure (McGregor et al., 1987; Willis et al., 1994; Clayton & Sawyer, 1999). It should, therefore, be possible to predict the lifetime distribution of tryptophans in different secondary structures, provided the value for χ_1 and χ_2 are known.

Table 7. *Comparison between calculated and measured lifetimes (ns)*

	Ha-ras p21(W32)		Tet repressor (W43)	
	Calculated τ	Measured τ	Calculated τ	Measured τ
τ_1	0.3 0.5	0.3	0.2 0.6	0.2
τ_2	1.8 2	1.8	2	2.8
τ_3	4.3	4.9	6	6.7

Changes in microconformations vs. a global conformational change upon BeF_3^- binding to p21(Y32W)-GDP

The p21-Y32W GDP bound variant has three lifetimes that do not change upon BeF_3^- binding, only the amplitude fraction of the middle lifetime increases from 0.16 to 0.71, while the amplitude fraction of the long lifetime decreases from 0.74 to 0.18 (Díaz et al., 1997a). The origin of the different lifetimes in p21-Y32W of W32 is either the existence of different microconformations of the tryptophan itself originated from different chi-angles or the existence of different conformations of the whole protein. At a first glance, it is possible that p21 has two conformations. One predominates when GDP is bound and is responsible for the long lifetime, and the other conformation dominates when GTP is bound and is responsible for the middle lifetime. But then the two lifetimes would have the same environment in both the GDP bound state and the GTP bound state, only the population of the different conformations would differ in both states. This is in contradiction with both the DAS (data not shown) and the quenching experiments that clearly indicate that both lifetimes have different environments in different states. This also means that the environment in itself is not responsible for the lifetimes of tryptophan. This is in agreement with the idea that the peptide bond is the major quencher for tryptophan fluorescence in proteins (Chen et al., 1996). If p21 switches from the GDP bound state to the GTP bound state, then there is a movement of the loop containing W32 putting the W32 in a solvent exposed environment. However, since the loop moves as a rigid body (Díaz et al., 1997b), there is no change in the relative conformation of the tryptophan toward the backbone of the loop, resulting in the same fluorescence lifetimes. The environment is indeed responsible for the probability of populating a possible conformation, in the GDP bound state the longest lifetime dominates and in the GTP bound state the middle lifetime dominates. The fact that the quenching data can be described by simple Stern Volmer behavior with constant amplitudes proves that these amplitudes are not kinetically determined.

Conclusion

The only relevant quenchers in proteins are the disulfide bridge, the amino acid side chains of protonated histidine, cysteine, maybe tyrosine, and the carbonyl carbon of the peptide bond (Vos & Engelborghs, 1994; Chen et al., 1996; Hennecke et al., 1997; Chen & Barkley, 1998). This means that the peptide bond is the only quencher that always influences the lifetimes of tryptophan and in some cases it is also the only one. The different fluorescence lifetimes of W57 (of NSCP) and W32 (of P21) can be explained as originating from different conformations of tryptophan with different distances between atom CE3 of tryptophan and the carbonyl carbon atom of the peptide bond. This mechanism of quenching by electron transfer is probably the main feature determining the lifetime of tryptophan in the absence of other pronounced quenchers. For an absolute proof, rigid molecules with a well-defined distance and orientation might be necessary, or peptide analogs with a missing tryptophan carbonyl.

Materials and methods

Materials

Isopropyl β-D-thiogalactoside (IPTG) was obtained from Promega (Madison, Wisconsin). $MgCl_2$ and EDTA were purchased from

Janssen Chimica (Beerse, Belgium). $CaCl_2$ was obtained from Riedel de Haen (Seelze, Germany), GuHCl was obtained from Fluka (Buchs, Switzerland), and N-acetyltryptophanamide and EGTA were obtained from Sigma Chemical Co. (St. Louis, Missouri). The buffer solution of NSCP was 50 mM Tris-HCl pH 7.5. The ionic strength of the solutions was always 0.2 M adjusted with KCl. The buffer of p21 contained 64 mM Tris, 50 mM HCl, 1 mM NaN_3, 1 mM dithioerythritol (DTE), 0.6 mM EDTA, 10 μM nucleotide (GDP), 1 mM $MgCl_2$, pH 7.2, containing different amounts of KHF_2 and $BeSO_4$, calculated using the complexing constants for Be^{+2} and F^- (Mesmer & Baes, 1969) to obtain free concentrations of BeF_3^- ranging from 0 to 87.7 mM. All buffer reagents were of analytical grade and were obtained from either Sigma, Janssen Chimica, ICN (Aurora, Ohio), or Fluka. All solutions were filtered through a 0.22 μm filter (Millipore Co.) and were spectroscopically pure. All the restriction endonucleases and Klenow polymerase were obtained from either New England Biolabs (Beverly, Massachusetts) or Boehringer Mannheim (Mannheim, Germany). The DNA purification kits were from Diagen GmbH (Düsseldorf, Germany).

Mutagenesis of NSCP

For expression of NSCP and its mutants, the plasmid pET22b(+) was used (Studier et al., 1990), into which the NSCP WT or mutant genes were prepared either by polymerase chain reaction or by cassette mutagenesis in the plasmid pNDner06 (Dekeyzer et al., 1994) and subsequently transferred in the pET22b(+), resulting in pETNSCP (van Riel, 1997). In this plasmid the NSCP gene is under control of the strong T7 promoter. Site-directed mutagenesis was performed according to Dekeyzer et al. (1994). The following oligonucleotides were used:

W4F:

5′-GGGGCATATGTCAGATCTC**TTC**GTTCAGAAAATGAAGACCTACTTC-3′

Nde I

W170F:

5′-CCCCAAGCTTACACAAGCGGGCC**GAA**GAATACTTTGTT-3′

Hind III

R25D: 5′-TAGATTCGAAGTCCATA**TC**CGTGATAGCACC-3′

D58R: R: 5′-GAAGTTG**CG**CCAGACGCCGGTGAG-3′

F: 5′-CGGCGTCTGG**CG**CAACTTCCTCAC-3′

The mutation W57F was made by cassette mutagenesis with the following cassette:

5′-CGGCGTC**TTC**GACAACTTCCTCAC-3′

3′-GTGGCCGCAG**AAG**CTCTTGAAGGTGTGCCGG-5′

which has restriction sites for BglI and EaeI.

Mutants where identified by restriction analysis and the mutated genes were entirely sequenced using the ABI PrismTM Big Dye Terminator Cycle Sequencing Ready Reaction system (Perkin Elmer, Foster City, California).

Expression and purification of NSCP

The *Escherichia coli* strain Bli5 (Bl21(DE3) + pDIA17) (Chang & Cohen, 1978; Studier & Moffat, 1986; Raleigh et al., 1988; Munier et al., 1991) was transformed by electroporation with the pETNSCP plasmids. Cells were then treated as described by Dekeyzer et al. (1994). The difference in negative charges between the Ca^{2+} and the apo state of the protein was used to purify NSCP. In a first stage, NSCP in the presence of Ca^{2+} was isolated from the other cell proteins by anion exchange chromatography (DEAE, Fast-Flow, Pharmacia, Uppsala, Sweden). This was repeated but with adjusting to 5 mM EGTA (apo conformation). In a last step, NSCP was purified on a Hiload Superdex 75 prepgrade 16/60 column (Pharmacia). To purify the NSCP W4-170F/R25D/D58R variant, an additional step was required before the anion exchange chromatography because this variant was only expressed as inclusion bodies. The inclusion bodies were isolated by sucrose gradient centrifugation (Vandenbroeck et al., 1993). They were subsequently denatured by 6 M Gu·HCl in presence of 5 mM EGTA at 37 °C during 15 h, and renatured by dialysis against 4 L 20 mM Tris-HCl, pH 7.5, 2 mM $CaCl_2$. The subsequent steps in the purification procedure were as with the other mutants except that the EGTA step was omitted. All NSCP variants were ≥99% pure as judged by Coomassie stained SDS gels. All the variants where stored with 2 mM $CaCl_2$. The apo form was made by adding EGTA and EDTA to a 10mM concentration each. The Mg^{2+} form was made by adjusting the apo form solution to 20 mM $MgCl_2$.

Mutagenesis and purification of p21

The Y32W mutant of p21 was produced and purified as described in Tucker et al. (1986) using a *ptac E. coli* expression system kindly donated by Prof. Dr. Alfred Wittinghofer (Max-Plank Institut für Molekulare Physiologie, Dormund, Germany). Its functionality was checked by the nucleotide binding assay (Tucker et al., 1986).

GDP-bound Ha-*ras*-p21 was prepared by a chromatography in a cold Sephadex G-25 column equilibrated in the GDP containing buffer. The concentrations of the samples were measured (Bradford, 1976) using bovine serum albumin as standard.

Steady-state fluorescence

Steady-state fluorescence was measured with a SPEX spectrofluorometer (Fluorolog 1691, Spex Industries, Edison, New Jersey, V.S.) with excitation and emission slits providing a bandpass of 7.2 and 3.6 nm, respectively. Spectra are corrected for the wavelength dependence of the emission monochromator and the photomultiplier and also by subtracting background intensities of the buffer solution. The cuvette holder was thermostated at 22 °C. The excitation wavelength was 295 nm to ensure that the measured fluorescence is only due to tryptophyl fluorescence.

UV absorption

UV absorption was measured on a Uvikon Kontron 940 spectrophotometer. The molar absorption coefficients at 295 nm are calculated by taking the ratio of the absorbance at 295 nm and at 280 nm, multiplied by the molar absorption coefficients at 280 nm, which was determined according to the method of Mach et al. (1992).

Fluorescence lifetime data

Fluorescence lifetime data were determined using an automated multifrequency phase fluorometer. The instrument is similar to the one described by Lakowicz et al. (1985), except for the use of a high-gain photomultiplier (Hamamatsu H5023) instead of a microchannel plate. The detection part is described by Vos et al. (1997). The excitation source consists of a mode-locked titanium-doped sapphire laser (Spectra Physics Tsunami) pumped by a Beamlok 2080 Ar^+-ion laser (Spectra Physics 2080). After frequency-tripling (Spectra Physics GWU), the excitation wavelength is 295 nm. A single harmonic component of the exciting light pulse train is first converted to an intermediate frequency of 455 kHz via external cross-correlation, and further filtered and amplified. The phase shift is measured in the low frequency domain (700 Hz) using a second cross-correlation step. In this way, fluorescence lifetime measurements are performed by measuring the phase shift of the modulated emission at 50 frequencies ranging from 1.6 MHz to about 1 GHz. N-Acetyltryptophanamide (in water filtered by the milliQ-system (Millipore)) with a fluorescence lifetime of 3.059 ns or p-terphenyl in cyclohexane with a lifetime of 1.04 ns (Desie et al., 1986) was used as a reference fluorophore. The measured phase shifts ϕ at a modulation frequency ω of the exciting light are related to the fluorescence decay in the time domain $I(t)$:

$$I(t) = \sum_i a_i \exp\left(\frac{-t}{\tau_i}\right) \tag{6}$$

where a_i is the amplitude of the fluorescence signal of the component with lifetime τ_i, by means of the following equation (Weber, 1981):

$$\tan\phi(\omega) = \frac{S(\omega)}{G(\omega)} \tag{7}$$

where $S(\omega)$ and $G(\omega)$ are the sine and the cosine Fourier transforms of $I(t)$:

$$S(\omega) = \sum_i f_i \frac{\omega\tau_i}{1+\omega^2\tau_i^2},$$

$$G(\omega) = \sum_i f_i \frac{1}{1+\omega^2\tau_i^2}, \tag{8}$$

and f_i the intensity contribution of the component with lifetime τ_i($f_i = a_i{\cdot}\tau_i/\sum_i a_i{\cdot}\tau_i$).

Data analysis was performed using a nonlinear least-squares algorithm (Bevington, 1969). Several statistical techniques were used in the fitting procedure as described by Clays et al. (1989). Measurements performed at different emission wavelengths were analyzed simultaneously with global analysis (GLOBALS UNLIMITED™, University of Illinois, Urbana, Illinois) to increase the resolution of the lifetimes and the corresponding amplitudes (Beechem et al., 1983). Phase data were fitted using the modified Levenberg–Marquardt algorithm (More & Sorensen, 1983) assuming fluorescence lifetimes that are independent of the emission wavelength and a variable amplitude ratio.

Quantum yields were determined relative to tryptophan in water according to the method of Parker and Rees (1960):

$$Q_{Prot} = \frac{\int I_{Prot} A_{\mathrm{Trp}}}{\int I_{\mathrm{Trp}} A_{Prot}} Q_{\mathrm{Trp}} \tag{9}$$

where $\int I$ is the integrated intensity over the wavelength region 300–450 nm, A is the absorbance at 295 nm, and the quantum yield Q_{Trp} for tryptophan in water is taken as 0.14 (Kirby & Steiner, 1970).

Decay associated spectra

Decay associated spectra are constructed by multiplying the intensity fraction with the intensity of the emission spectra at the respective wavelength (Ross et al., 1981). A lognormal function (Burstein & Emelyanenko, 1996) is fitted to the associated intensities to obtain the decay associated spectra.

$$I(\lambda) = I_m \exp\left[\frac{\ln 2}{\ln^2\rho}\ln^2\left(\frac{(a-1/\lambda)}{(a-1/\lambda_m)}\right)\right]. \tag{10}$$

Here, $I_m = I(\lambda_m)$ is the maximal fluorescence intensity; λ_m is the wavelength of the band maximum; $\rho = (1/\lambda_m - 1/\lambda_-)/(1/\lambda_+ - 1/\lambda_m)$ is the band asymmetry parameter; $a = 1/\lambda_m + (1/\lambda_+ - 1/\lambda_-)\rho/(\rho^2 - 1)$ is the function limiting point; $\lambda_+ = 10^7/(0.830{\cdot}10^7/\lambda_m + 7{,}071)$ and $\lambda_- = 10^7/(1.1768{\cdot}10^7/\lambda_m - 7{,}681)$ are the wavelength positions of half-maximal amplitudes.

The average radiative rate constant is calculated by dividing the quantum yield by a wavelength independent amplitude average lifetime (Sillen & Engelborghs, 1998):

$$\langle k_r\rangle = \frac{Q}{\Sigma\tau_i\alpha_i}. \tag{11}$$

Here, α_i is a wavelength independent amplitude fraction and is defined as (Willis & Szabo, 1992; Sillen & Engelborghs, 1998)

$$\alpha_i = \frac{\int I_{0i}(\lambda)\,d\lambda}{\sum_{l=1}^{l=n}\int I_{0l}(\lambda)\,d\lambda} = \frac{\int I_{0i}(\lambda)\,d\lambda}{\int I_0(\lambda)\,d\lambda}. \tag{12}$$

The fluorescence intensity at time zero $I_0(\lambda)$ of each lifetime is integrated over the wavelength region 300–450 nm and then normalized.

Energy map of NSCP

To characterize the possible conformations of tryptophan, a minimum perturbation map is calculated (Silva & Prendergast, 1996). Minimum perturbation mapping of W57 was performed using the CHARMM22 package (Brooks et al., 1983). Map calculation used the all-hydrogen CHARMM22 parameter and topology file. Minimum perturbation maps (Haydock, 1993) are calculated by fixing the Trp side chain at a particular χ_1, χ_2 point and allowing the residues nearby Trp to conformationally relax so as to achieve an

energy minimization, where all the other residues are fixed to their crystallographic coordinates. The nearby residues included residues 22–29 and 52–70. The minimization procedure, used at each Trp dihedral point, was 100 steps by steepest descent method, 1,000 steps with a tolerance of 0.1 by the Powell method. This is repeated in 10° steps over the whole angular space of χ_1 and χ_2. Throughout this paper, χ_1 is defined by the bond connectivity N-C_α-C_β-C_γ and χ_2 is defined by the bond connectivity C_α-C_β-C_γ-$C_{\delta 1}$. These maps display areas where Trp is in an energetically favored position.

Molecular dynamics of NSCP

All the MD calculations of NSCP were performed using CHARMM22 (all hydrogens) and with the molecule in vacuum. The starting structure is the X-ray structure containing three Ca^{2+} ions (Vijay-Kumar & Cook, 1992) obtained from the Brookhaven Protein Data Bank (Bernstein et al., 1977). This structure is energy minimized by a 2,000 step conjugate gradient minimization algorithm. From this energy minimized structure, the χ_1 and χ_2 angle of Trp57 are set at the appropriate values. These structures are again energy minimized with 1,000 steps. These structures are warmed up to 300 K in 20 ps and then equilibrated during 50 ps. Consequently, a normal MD simulation of 50 ps was done to monitor the χ_1 and χ_2 angles of Trp57.

MD simulation of p21

The three-dimensional X-ray structure of p21 was obtained from the Brookhaven Protein Data Bank (Bernstein et al., 1977). The GROMOS 87 (Van Gunsteren & Berendsen, 1987) package was obtained from Biostructure S.A. (France). The input files for the GROMOS 87 package were generated using the program WHATIF (Vriend, 1990), which was also used to make the mutations in the three-dimensional X-ray structure. The structures were placed in a truncated octahedral box of SPC water (Berendsen et al., 1981) with the counter ions (Cl^- and Na^+), where a minimum distance of 7 Å was kept between the protein and the border of the box. The energies of the protein and the water were then minimized for 500 steps using a steepest descent algorithm (Levitt & Lifson, 1969). The velocities of the atoms were assigned following a Maxwellian velocity distribution at 100 K. The system was warmed up to 300 K in two consecutive steps of 1.3 ps in total, and a free MD simulation was performed for 200 ps using a constant pressure of 1 atm and a constant temperature of 300 K. The temperature of the protein and the solvent are separately coupled to a water bath (Berendsen et al., 1984) using a coupling constant of 0.1 ps. The pressure was kept constant by coupling to an external pressure bath (Berendsen et al., 1984) with a coupling constant of 0.5 ps. The conditions of the MD simulation were the following: the time step employed was 2 fs, the integration of the equations of motion and energy were done using a leap frog algorithm included in the GROMOS package, the bond lengths were constrained using the SHAKE routine (Ryckaert et al., 1977), and a cutoff of 8 Å was used for nonbonded interactions (van der Waals interactions), and of 11 Å for the electrostatic interactions. For analysis, the coordinates were saved every ps. The calculations were performed using a Silicon Graphics Indigo 2 workstation equipped with a MIPS R10000 processor. The data were analyzed using the programs WHATIF[42] and SIMLYS (Krüger et al., 1991).

Fluorescence quenching of p21 with Cu^{2+} and I^-

The KI stock solution was prepared with 25 mM $Na_2S_2O_3$ to prevent the formation of I_2. The quenching of p21 with increasing amounts of quencher was performed by adding aliquots of a stock solution of KI (5 M) or $CuCl_2$ (25 mM) to the cuvette containing the protein after which the changes in the fluorescence lifetimes and corresponding amplitude fractions were monitored. Fluorescence lifetime as function of quencher concentration $[Q]$ was fitted by the classical Stern–Volmer equation

$$\frac{1}{\tau} = \frac{1}{\tau_0} + k_q[Q] \tag{13}$$

where $\tau_0(\tau)$ is the lifetime in absence (presence) of quencher.

Calculation of the nonradiative rate constant

The nonradiative rate constant (k_{nr}) is calculated by following equation:

$$k_{nr} = \frac{1}{\tau} - k_r \tag{14}$$

where k_r is the radiative rate constant, which is calculated as shown before, and τ is the fluorescence lifetime.

Acknowledgments

This project was supported by a research grant from the Fund for Scientific Research G.0242.96 (Belgium/Flanders). We thank Prof. Dr. Guido Volckaert for providing laboratory support for the constructions and expression of the mutants, Lotte Delfosse and Tania Braem for technical assistance, Dr. Johan Robben for support and suggestions with cloning techniques, and Dr. Peter Krüger for useful discussions.

References

Adari H, Lowy DR, Willumsen BM, Der CJ, McCormick F. 1988. Guanosine triphosphatase activating protein (GAP) interacts with the ras-p21 effector binding domain. *Science 240*:518–521.

Antonini PS, Hillen W, Ettner N, Hinrichs W, Fantucci P, Doglia SM, Bousquet J-A, Chabbert M. 1997. Molecular mechanics analysis of tet repressor Trp-43 fluorescence. *Biophys J 72*:1800–1811.

Beechem JM, Knutson JR, Ross JBA, Turner BW, Brand L. 1983. Global resolution of heterogeneuos decay by phase modulation fluorometry: Mixtures and proteins. *Biochemistry 22*:6054–6058.

Berendsen HJC, Postma JPM, Van Gunsteren WF, Dinola A, Haak JR. 1984. Molecular dynamics with coupling to an external bath. *J Chem Phys 81*:3684–3690.

Berendsen HJC, Postma JPM, Van Gunsteren WF, Hermans J. 1981. Interaction models for water in relation to protein hydratation. In: Pullman B, ed. *Intramolecular forces*. Dordrecht: Reidel. pp 331–342.

Bernstein FC, Koetzle TF, Williams GJB, Meyer EF Jr, Brice MD, Rodgers JR, Kennard O, Shimanouchi T, Tasumi M. 1977. The Protein Data Bank: A computer-based archival file for macromolecular structures. *J Mol Biol 112*:535–542.

Bevington PR. 1969. Gradient-expansion algorithm. In: *Data reduction and error analyses for the physical sciences*. New York: McGraw-Hill. pp 235–240.

Bradford MM. 1976. A rapid and sensitive method for the quantitation of microgram quantities of protein utilizing the principle of protein-dye binding. *Anal Biochem 72*:248–254.

Brooks BR, Bruccoleri RE, Olafson BD, States DJ, Swaminathan S, Karplus M. 1983. CHARMM: A program for macromolecular energy, minimization and dynamics calculations. *J Comput Chem 4*:187–217.

Burstein EA, Emelyanenko VI. 1996. Log-normal description of Fluorescence spectra of organic fluorophores. *Photochem Photobiol 64*:316–320.

Callis PR, Burgess BK. 1997. Tryptophan fluorescence shifts in proteins from hybrid simulations: An electrostatic approach. *J Phys Chem 101*:9429–9432.

Chang ACY, Cohen SN. 1978. Construction and characterization of amplifiable multicopy DNA cloning vehicles from the P15A cryptic miniplasmid. *J Bacteriol 1*:1141–1156.

Chen Y, Barkley MD. 1998. Toward understanding tryptophan fluorescence in proteins. *Biochemistry 37*:9976–9982

Chen Y, Liu B, Yu H-T, Barkley MD. 1996. The peptide bond quenches indole fluorescence. *J Am Chem Soc 11*:9271–9278.

Clays K, Jannes J, Engelborghs Y, Persoons A. 1989. Instrumental and analysis improvement in multifrequency phase fluorometry. *J Phys E Sci Instrum 22*:297–305.

Clayton AHA, Sawyer WH. 1999. Tryptophan rotamer distributions in amphipathic peptides at a lipid surface. *Biophys J 76*:3235–3242.

Collins JH, Cox JA, Theibert JL. 1988. Amino acid sequence of a sarcoplasmic calcium-binding protein from the sandworm *Nereis diversicolor*. *J Biol Chem 263*:15378–15385.

Dahms TES, Willis KJ, Szabo AG. 1995. Conformational heterogeneity of tryptophan in a protein crystal. *J Am Chem Soc 117*:2321–2326.

Dekeyzer N, Engelborghs Y, Volckaert G. 1994. Cloning, expression and purification of a sarcoplasmic calcium-binding protein from the sandworm *Nereis diversicolor* via a fusion product with chloramphenicol acetyltransferase. *Protein Eng 7*:125–130.

Desie G, Boens N, De Schryver FC. 1986. Study of the time-resolved tryptophan fluorescence of crystalline α-chymotrypsin. *Biochemistry 25*:8301–8308.

Díaz JF, Sillen A, Engelborghs Y. 1997a. Equilibrium and kinetic study of the conformational transition towards the active state of Ha-ras-p21, induced by the binding of BeF_3^- to the GDP-bound state, in the absence of GAP's. *J Biol Chem 272*:23138–23143.

Díaz JF, Wroblowski B, Schlitter J, Engelborghs Y. 1997b. Calculation of pathways for the conformational transition between the GTP- and GDP-bound states of the Ha-ras-p21 protein: Calculations with explicit solvent simulations and comparison with calculations in vacuum. *Proteins Struct Funct Genet 28*:434–451.

Gordon HL, Jarrell HC, Szabo AG, Willis KJ, Somorjai RL. 1992. Molecular dynamics simulations of the conformational dynamics of tryptophan. *J Phys Chem 96*:1915–1921.

Gray HB, Winkler JR. 1996. Electron transfer in proteins. *Annu Rev Biochem 65*:537–561.

Harris D, Hudson B. 1990. The photophysics of tryptophan in bacteriophage T4 lysozyme. *Biochemistry 29*:5276–5285.

Haydock C. 1993. Protein side chain rotational isomerisation: A minimum perturbation mapping study. *J Chem Phys 98*:8199–8214.

Hennecke J, Sillen A, Huber-Wunderlich M, Engelborghs Y, Glockshuber R. 1997. Quenching of the tryptophan fluorescence by the active-site disulfide bridge in the dsbA protein from *Escherichia coli*. *Biochemistry 36*:6391–6400.

Hudson BS. 1999. An ionization/recombination mechanism for complexity of the fluorescence of tryptophan in proteins. *Acc Chem Res 32*:297–300.

Kirby EP, Steiner RFS. 1970. The influence of solvent and temperature upon the fluorescence of indole derivatives. *J Phys Chem 74*:4480–4490.

Kraulis PJ. 1991. MOLSCRIPT: A program to produce both detailed and schematic plots of protein structures. *J App Crystallogr 24*:946–950.

Kretsinger RH, Nockolds CE. 1973. Carp muscle calcium-binding protein. II. Structure determination and general description. *J Biol Chem 248*:119–174.

Krüger P, Lüke M, Szameit A. 1991. SIMLYS—A software package for trajectory analysis of molecular dynamics simulations. *Comput Phys Commun 62*:371–380.

Lakowicz JR, Laczko G, Gryczinski I. 1985. 2-GHz frequency-domain fluorometer. *Rev Sci Instrum 57*:2499–2506.

Levitt M, Lifson S. 1969. Refinement of protein conformations using a macromolecular energy minimization procedure. *J Mol Biol 46*:269–279.

Mach H, Middaugh CR, Lewis RV. 1992. Statistical determination of the average values of the extinction coefficients of tryptophan and tyrosine in native proteins. *Anal Biochem 200*:74–80.

Marcus RA, Sutin N. 1985. Electron transfer in chemistry and biology. *Biochim Biophys Acta 811*:265–322.

McGregor MJ, Suhail A, Sternberg MJE. 1987. Analysis of the relationship between side-chain conformation and secondary structure in globular proteins. *J Mol Biol 198*:295–310.

Mesmer RE, Baes CF. 1969. Fluoride complexes of beryllium(II) in aqueous media. *Inorg Chem 8*:618–626.

More JJ, Sorensen DC. 1983. Computing a trust region step. *SIAM J Sci Stat Comput 4*:553–572.

Munier H, Gilles A-M, Glaser P, Krin E, Danchin A, Sarfati R, Bârzu O. 1991. Isolation and characterization of catalytic and calmodulin-binding domains of *Bordetella pertussis* adanylate cyclase. *Eur J Biochem 196*:469–474.

Pai EF, Krengel U, Petsko GA, Goody RS, Kabsh W, Wittinghofer A. 1990. Refined crystal structure of the triphosphate conformation of H-ras-p21 at 1.35 Å resolution: Implications for the mechanism of GTP hydrolysis. *EMBO J 9*:2351–2359.

Parker CA, Rees WT. 1960. Corrections of fluorescence spectra and the measurement of fluorescence quantum efficiency. *Analyst 85*:587–600.

Raleigh EA, Murray NE, Revel H, Blumenthal RM, Westaway D, Reith AD, Rigby PW, Elhai J, Hanahan D. 1988. McrA and McrB restriction phenotypes of some *E. coli* strains and implications for gene cloning. *Nucleic Acids Res 16*:1563–1575.

Rensland H, John J, Linke R, Simon I, Schlichting I, Wittinghofer A, Goody RS. 1995. Substrate and product structural requirements for binding of nucleotides to H-ras p21: The mechanism of discrimination between guanosine and adenosine nucleotides. *Biochemistry 34*:593–599

Ross JA, Schmid CJ, Brand L. 1981. Time-resolved fluorescence of the two tryptophans in horse liver alcohol dehydrogenase. *Biochemistry 20*:4369–4377.

Ryckaert JP, Ciccotti G, Berendsen HJC. 1977. Numerical integration of cartesian equations of motion of a system with constrains: Molecular dynamics of n-alkanes. *J Comput Phys 23*:327–341.

Schlitter J, Engels M, Krüger P. 1994. Targeted molecular dynamics: A new approach for searching pathways of conformational transitions. *J Mol Graphics 12*:84–89.

Sillen A, Engelborghs Y. 1998. The correct use of "average" fluorescence parameters. *Photochem Photobiol 67*:475–486.

Sillen A, Hennecke J, Roethlisberger D, Glockshuber R, Engelborghs Y. 1999. Fluorescence quenching in the DsbA protein from *Escherichia coli*. The complete picture of the excited state energy pathway and evidence for the reshuffling dynamics of the microstates of tryptophan. *Proteins Struct Funct Genet 37*:253–263.

Silva ND, Prendergast FG. 1996. Tryptophan dynamics of the FK506 binding protein: Time-resolved fluorescence and simulations. *Biophys J 70*:1122–1137.

Strickler SJ, Berg RA. 1962. Relationship between absorption intensity and fluorescence lifetime of molecules. *J Chem Phys 37*:814–822.

Studier FW, Moffat BA. 1986. Use of bacteriophage T7 RNA polymerase to direct selective high-level expression of cloned genes. *J Mol Biol 189*:113–130.

Studier FW, Rosenberg AH, Dunn JJ, Dubendorf JW. 1990. Use of T7 polymerase to direct expression of cloned genes. *Methods Enzymol 185*:60–89.

Szabo AG, Faerman C. 1992. Dilemma of correlating fluorescence quantum yields and intensity decay times in single tryptophan mutant proteins. *SPIE 1640*:70–80.

Tong LA, de Vos AM, Milburn MV, Kim SH. 1991. Crystal structures at 2.2 Å resolution of the catalytic domains of normal ras protein and an oncogenic mutant complexed with GDP. *J Mol Biol 217*:503–516.

Tucker J, Sczakiel G, Feuerstein J, John J, Goody RS, Wittinghofer A. 1986. Expression of p21 proteins in *Escherichia coli* and stereochemistry of then nucleotide-binding site. *EMBO J 5*:1351–1358.

Valeur B, Weber G. 1977. Resolution of the fluorescence excitation spectrum of indole into the ^1L_a and ^1L_b excitation bands. *Photochem Photobiol 25*:441–444.

Vandenbroeck K, Martens E, D'Andrea S, Billiau A. 1993. Refolding and single-step purification of porcine interferon-gamma from *Escherichia coli* inclusion bodies. Conditions for reconstitution of dimeric IFN-gamma. *Eur J Biochem 215*:481–486.

Van Gunsteren WF, Berendsen HJC. 1987. Program system GROMOS 87. Biomos Biomolecular Software b.v. Laboratory of Physical Chemistry University of Groningen.

van Riel A. 1997. Karakterisatie van het Ca^{2+}-bindingsmechanisme van *Nereis* SCP met behulp van plaatsgerichte mutagenese [PhD thesis]. KULeuven, Leuven.

Vijay-Kumar S, Cook WJ. 1992. Structure of a sarcoplasmic calcium-binding protein from *Nereis diversicolor* refined at 2.0 Å resolution. *J Biol Chem 224*:413–426.

Vos R, Engelborghs Y. 1994. A fluorescence study of tryptophan-histidine interaction in the peptide anantin and in solution. *Photochem Photobiol 60*:24–32.

Vos R, Strobbe R, Engelborghs Y. 1997. Gigahertz phase fluorometry using a fast high-gain photomultiplier. *J Fluorescence 7*:33S–35S.

Vriend G. 1990. WHAT IF: A molecular modeling and drug design program. *J Mol Graphics 8*:52–56.

Weber G. 1981. Resolution of the fluorescence lifetimes in a heterogeneous system by phase and modulation measurements. *J Phys Chem 85*:949–953.

Wierzchowski KL. 1997. Intramolecular electron transfer between tryptophan radical and tyrosine in oligoproline-bridged model peptides and egg-white lysozyme. *Acta Biochim Polon 44*:627–644

Willis KJ, Neugebauer W, Sikorska M, Szabo AG. 1994. Probing α-helical secondary structure at a specific site in model peptides via restriction of tryptophan side-chain rotamer conformation. *Biophys J 66*:1623–1630

Willis KJ, Szabo AG. 1992. Conformation of parathyroid hormone: Time-resolved fluorescence studies. *Biochemistry 31*:8924–8931.

Wittinghofer A, Pai EF. 1991. The structure of ras protein: A model for a universal molecular switch. *TIBS 16*:382–387.